J Mater Sci (2009) 44:4162–4168
DOI 10.1007/s10853-009-3617-2

Influence of copper on the microstructure of sol–gel titanium oxide nanotubes array

S. López-Ayala · M. E. Rincón · H. Pfeiffer

Received: 27 January 2009 / Accepted: 18 May 2009 / Published online: 2 June 2009

Abstract The effect of copper addition in the microstructure of sol–gel titanium oxide (TiO_2) supported on anodic aluminum oxide (AAO) membranes is reported. Two deposition methods based on immersion and flow techniques were used for the coating of the porous AAO membrane. Copper-free membranes were studied as a function of different ratios of H^+/Ti, H_2O/Ti, selecting the most appropriate for the sensitization with copper. For copper-doped TiO_2 arrays, the presence of copper causes the reduction of grain size and enhances titania deposition inside the AAO pores, although no clear tendency with copper content was found. The formation of copper-doped titania nanotubes was validated after dissolving the AAO membranes, finding a deposition-dependent stability in the Cu-doped materials. Titania and Cu-doped titania nanotubes analyzed as colloidal solutions show band gaps substantially shifted to the red in comparison to the direct band gap of near-spherical colloidal materials. These arrays are important for photocatalysis and for the development of third generation photovoltaic devices.

Introduction

One-dimensional nanostructures have received much attention due to their unique properties and potential applications. Among the various methods implemented for fabrication of one-dimensional materials, deposition from solution has several advantages, such as low cost, scaling to various sizes and shapes, and stoichiometric control [1, 2]. Still, the challenge to understand and control the chemistry at the molecular level, and the geometry and size of the particles elaborated continue to be an intense area of research. Among the various nanotubes synthesized, TiO_2 nanotubes arrays have been obtained by electrochemical anodization and by combining sol–gel techniques with anodic aluminum oxide (AAO) templates [1–11]. Work on TiO_2-based nanotubes with improved properties follow the promising results of titania nanoparticles, where the inclusion of doping agents has enhanced full spectrum photoresponse [11], photocatalytic/catalytic properties [12–15], and ferromagnetism [16]. In particular, the low cost and availability of Cu and its activity as a catalyst in many oxidation and reduction reactions, make its use as a doping agent for titania matrices very attractive [12, 13, 17–26].

Up to date, the science and engineering applications of highly ordered titania nanotube arrays seem remarkable, but as stated in a recent review by Mor et al., the work has just begun [11]. In this contribution, we study the influence of copper on the microstructure of Cu-doped TiO_2 nanotube arrays and the effect of two deposition techniques imposing different nucleation conditions during the sol–gel template synthesis. The immersion technique is dominated by strong capillary forces and most likely by the geometrical parameters of the pore and the critical nucleus (i.e., nucleation of the solid after hydrolysis/condensation) [26–28]. On the other hand, forcing the continuous flow of sol–gel solution through the pores of the AAO membrane significantly alters the dynamics of nucleation and growth in a way that could favor the formation of nanotubes with

S. López-Ayala · M. E. Rincón (✉)
Centro de Investigación en Energía-Universidad Nacional Autónoma de México, Apartado Postal 34, Temixco 62580, MOR, Mexico
e-mail: merg@cie.unam.mx

H. Pfeiffer
Instituto de Investigaciones en Materiales—Universidad Nacional Autónoma de México, Circuito exterior s/n, Cd. Universitaria, Del. Coyoacan, CP 04510 México, DF, Mexico

few defects and thicker walls, given that a relatively constant reactant concentration is obtained by the flow technique, in contrast to the concentration gradient formed in the immersion technique where the reactants inside the pores have to be replenished by diffusion. Previous reports on Cu-doped TiO_2 nanoparticles (17–20 nm) include those obtained via refined alkoxide sol–gel process [21, 23, 24, 26, 29], as well as those obtained by impregnation and co-precipitation methods and used in the catalytic and photocatalytic conversion of phenol, CO, CO_2, and NO [12–15, 19, 20, 25]. No reports were found on the synthesis and properties of Cu-doped TiO_2 nanotubes catalysts confined in an ordered matrix such as AAO templates.

Experimental details

Commercial AAO membranes (Anodisc 13, Whatman), with 13 mm diameter, 60 μm thickness, and 20 nm pore diameter were used as the templates. Titania *sols* were prepared by mixing either ethyl or isopropyl alcohol (Sigma-Aldrich) with 35 wt.% HCl (JT-Baker), water, and titanium (IV) isopropoxide (Sigma-Aldrich), keeping the mixture at ambient conditions under strong stirring; *sols* containing Cu ions were obtained by adding $CuCl_2$ (Sigma-Aldrich) in the desired proportions. Filling the AAO templates with titania or Cu-doped titania *sols* was accomplished by either immersing the membranes into the appropriate *sol*, or by pumping the *sol* into the membranes placed at the bottom of 10 mL adapted syringes. A close system was implemented for better humidity control while the optimization of H_2O/Ti, H^+/Ti, type of alcohol, and deposition time, were pursued previous to doping with Cu. The details of these experimental trials are given in Table 1. Table 2 shows the composition of the copper containing *sols* used for the elaboration of Cu-doped TiO_2 nanotube arrays. The Cu/Ti molar ratio was varied in the range of 0.006–0.04 keeping other parameters constant (i.e., H^+/Ti = 0.13, H_2O/Ti = 1.2, ethanol/Ti = 45). The coated AAO templates were annealed in air at 450 °C for 1 h. For SEM and TEM analysis, the dissolution of AAO membranes in 5 wt. % NaOH solution was accomplished in 45 min in both TiO_2/AAO and TiO_2–Cu_xO/AAO membranes.

Scanning electron microscopy analyses (Stereoscan 440—Leyca Cambridge) were performed to determine the surface morphology of the samples elaborated. TEM images were obtained with a field emission transmission electron microscope (JEOL JEM-2010F FasTEM) working a 200 kV, after dispersing the AAO-free catalyst in ethanol and by dropping them onto a copper grid. The microstructure

Table 2 Molar ratios for the preparation of copper-doped titania sols used in the coating of AAO membranes by flow and immersion techniques

H^+/Ti	H_2O/Ti	C_2H_5OH/Ti	Cu/Ti	Flow/immersion time, h
0.13	1.2	45	0.000	3.5, 4.5, 5.5
0.13	1.2	45	0.006	3.5, 4.5, 5.5
0.13	1.2	45	0.020	3.5, 4.5, 5.5
0.13	1.2	45	0.040	3.5, 4.5, 5.5

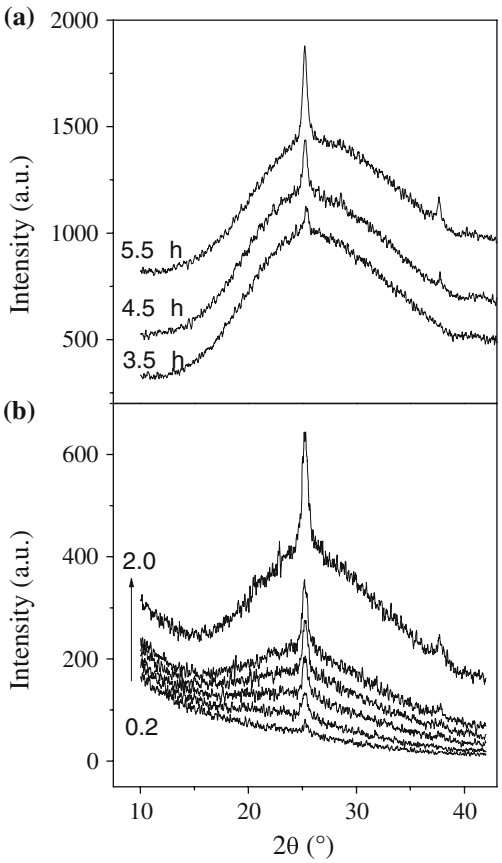

Fig. 1 XRD patterns of TiO_2–Cu_xO/AAO as a function of flow time (**a**) and grazing angle (**b**)

Table 1 Molar ratios for the preparation of titania sols used in the coating of AAO membranes by flow and immersion techniques

H^+/Ti	H_2O/Ti	C_3H_7OH/Ti	C_2H_5OH/Ti	Immersion time, h	Flow time, h	*Sol* description
0.05–0.15	1.2	45	–	–	–	Precipitates
0.05–0.18	1.9		45	3,4,6	–	Transparent sol
0.18–0.4	1.2	45	–	–	3, 4, 6	Transparent sol

and degree of surface coverage inside the AAO pores were investigated by X-ray diffraction studies (Rigaku Dmax 2200), using CuK_α radiation ($\lambda = 1.54$ Å) as the X-ray source, and Bragg-Brentano and grazing angle analysis configurations in the 2θ range of 10° to 70°. In contrast to the conventional Bragg-Brentano analysis, where X-ray penetration is of few millimeters causing the pattern to be dominated by the substrate (i.e., AAO membrane), the comparison of X-ray spectra at various grazing angle θ_i, allows for the differentiation of crystallites grown at the surface (spectra obtained at lower θ_i) from those grown in the bulk (spectra obtained at higher θ_i). In the case of a filled porous membrane, the increase in peak intensity with increasing grazing angle indicates the contribution of crystallites grown along the length (bulk) of the pore. If there is a decrease or constant value in peak intensity with increasing θ_i, that will be an indication of titania growth outside the AAO pores. The average crystal size was obtained from the most intense peak by means of the Scherrer equation [30], after correcting for FWHM instrumental error using lanthanun hexaboride powder as standard reference material. The optical transmittance of TiO_2 and Cu-doped TiO_2 films and powders was obtained with a Shimadzu UV-3101PC spectrophotometer in the wavelength interval of 250–2500 nm.

Results

Transparent and precipitate-free *sols* were obtained at relatively low H^+/Ti molar ratio in ethanol, in agreement with the findings reported by Anderson et al. [31]. Pumping these *sols* through AAO templates renders uniform deposits on the pore inner surface in closed systems. Figure 1 gives the structural characterization of Cu-doped TiO_2 supported on AAO membranes (TiO_2–Cu_xO/AAO) obtained by the flow method; here the increment in peak intensity with flow time can be observed in the conventional XRD analysis shown in Fig. 1a, while the trend of increasing peak intensity with increasing grazing angle indicative of homogeneous coating inside AAO pores is shown in Fig. 1b. The protruding background in the range from 15°

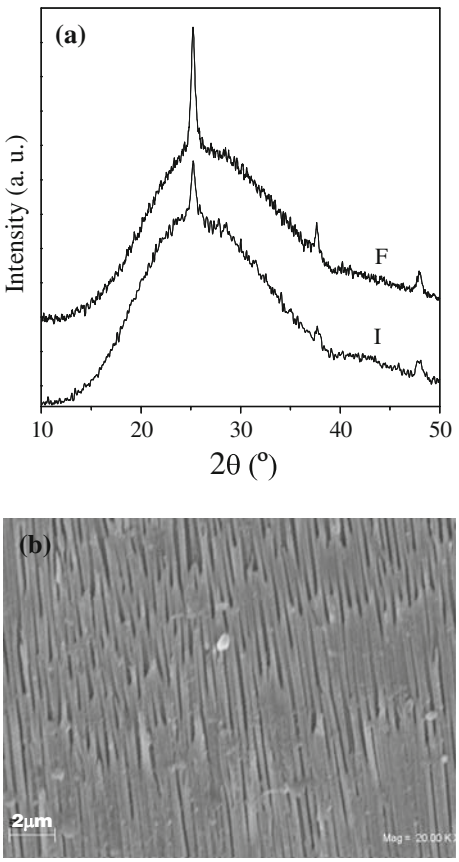

Fig. 2 (**a**) Conventional XRD patterns of TiO_2–Cu_xO/AAO obtained by the immersion (I) and flow (F) techniques. Arrays obtained at 5.5 h deposition time at the atomic (molar) ratios of: Cu/Ti = 0.0016, H^+/Ti = 0.13, H_2O/Ti = 1.2, ethanol/Ti = 45. (**b**) Typical cross-section SEM image

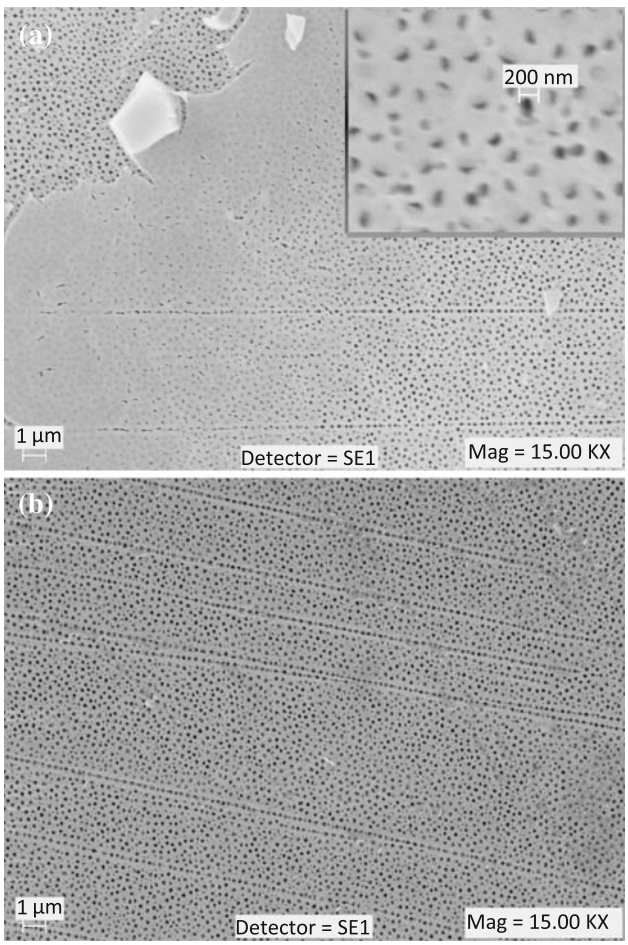

Fig. 3 SEM images of TiO_2–Cu_xO/AAO obtained at 5.5 h immersion time with Cu/Ti = 0.02 (**a**) and Cu/Ti = 0.04 (**b**)

to 40° corresponds to the XRD pattern of the AAO membrane and the sharper peaks to the main diffraction planes of the anatase phase. SEM images of these samples (not shown) indicates that up to 4 h flow time there is a gradual increase in pore filling that does not manifest as a unique nanotube wall thickness, but rather as a distribution of values given the broad pore size-distribution of commercial AAO templates. This make the estimated wall thickness difference of nanotubes formed at deposition times <4 h difficult to asses by SEM analysis. Above 4 h deposition time, most narrow AAO pores are completely filled and an outer titania layer begins to form being 100–200 nm thicker in samples obtained by flow. The comparison of copper-doped samples obtained at 5.5 h by the two deposition methods and annealed at the same conditions is shown in Fig. 2a. Here the conventional Brag-Brentano geometry was used to examine the samples and the lower peak intensity of those obtained by immersion suggest inferior titania content inside the pores, given that titania outlayers were removed by carefully rubbing the AAO surface. Figure 2b shows the typical cross-sectional image of coatings obtained by either technique where small pores appear completely filled and larger pores partially filled.

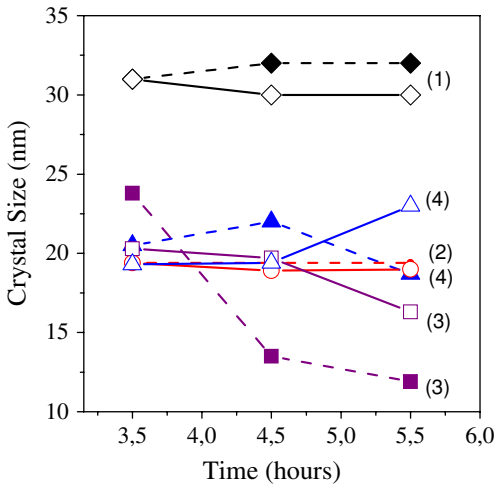

Fig. 4 Crystal size of titania and Cu-doped titania nanotube arrays obtained by the immersion (*solid line*) and flow techniques (*dashed lines*). (1) Cu/Ti = 0; (2) Cu/Ti = 0.006; (3) Cu/Ti = 0.02; (4) Cu/Ti = 0.04

The effect of Cu on titania deposition is illustrated in Fig. 3, where SEM images of TiO_2–Cu_xO/AAO membranes obtained by immersion at different Cu/Ti ratio show a more uniform but thinner coating when increasing the Cu/Ti ratio from 0.02 (Fig. 3a) to 0.04 (Fig. 3b); similar effects occur in samples obtained by flow. Thinning of the coating not necessarily correlates with the variation in crystallite size. Figure 4 shows the variation of crystallite size with respect to immersion/flow time and/or copper content and it is notorious that the larger crystals are obtained by immersion regardless of their thinner coatings.

Titania and copper-doped titania particles formed at long deposition times and obtained after the dissolution of AAO membranes are shown in Figs. 5 and 6. Figure 5a corresponds to TEM images of Cu-free TiO_2 nanotubes formed inside wide pores of AAO membranes by the immersion technique, and Fig. 5b to a magnified TEM image of Cu-doped TiO_2 nanorod formed also by immersion. The dark spots of Fig 5b were identified as small 5 nm CuO and $Cu(OH)_2$ clusters by FFT indexation of the lattice fringes. At lower magnification, SEM images show the dominance of tubular material but close inspection verifies the abundance of narrow nanowires. Additionally, the well-defined nanotube geometry of copper free titania obtained by the flow technique (Fig. 6a) switch to copper-doped titania sheets (Figs. 6b–c), particularly in Cu-doped nanotubes obtained by immersion.

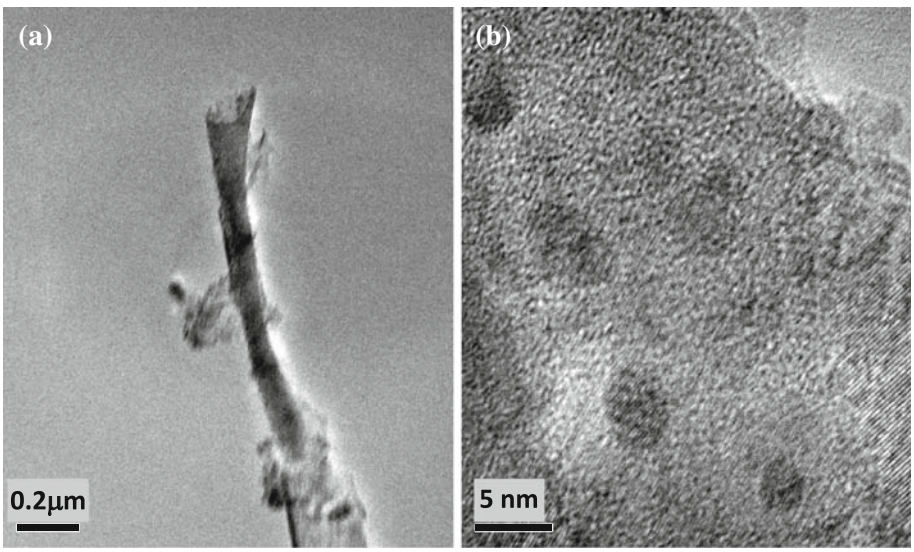

Fig. 5 TEM images of titania (**a**) and copper-doped titania particles (**b**) obtained by immersion

The optical characterization of titania and copper-doped titania films and powders is given in Fig. 7. The band gaps were calculated from the equations describing the optical absorption of direct ($n = 2$) and indirect ($n = 1/2$) transitions in crystalline materials [32]. The plot of $(\alpha dhv)^n$ vs. hv, where α is the absorption coefficient, d is the thickness of the absorbing layer, and hv is the photon energy, provides the value of band gap from extrapolation of the linear part of the curve near the onset of absorption. For titania and Cu-doped titania films deposited from sol–gel baths on Corning glass substrates (near spherical particles), no significant band gap shift is observed between copper-free and copper-doped materials, neither a clear tendency with copper content, in agreement with previous report [26]. For titania and Cu-doped titania nanotubes analyzed as colloidal solutions (Fig. 7b), the band gap is substantially shifted to the red in comparison to the near spherical particles presented in Fig. 7a.

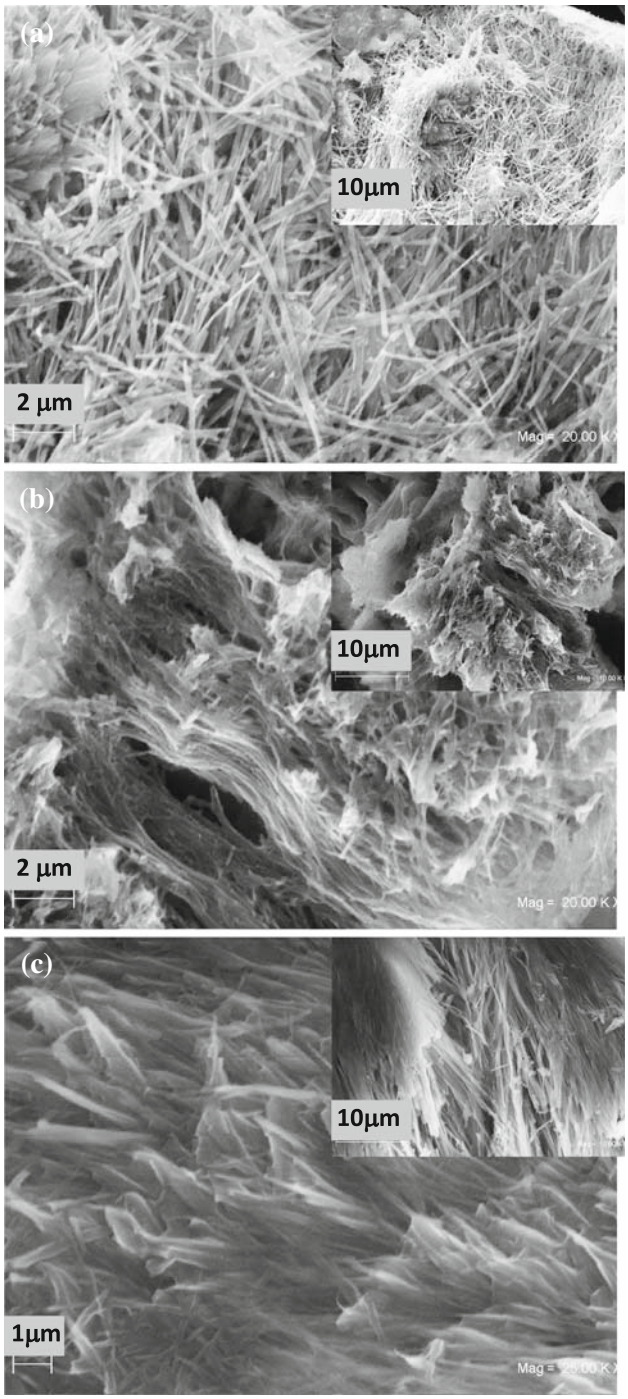

Fig. 6 SEM images of titania (**a**) and copper-doped titania particles (**b–c**) obtained after the dissolution of AAO membranes: (**a**) and (**c**) refer to deposits obtained by flow, and (**b**) to materials obtained by immersion

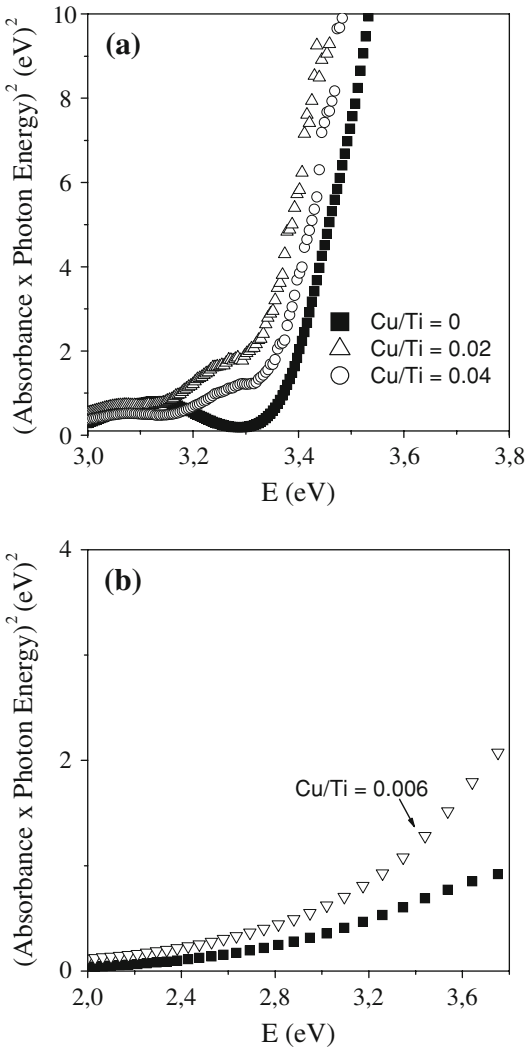

Fig. 7 Optical band gap determination assuming direct transitions: (**a**) titania and Cu-doped titania films deposited on Corning glass substrates; (**b**) titania and Cu-doped titania nanotubes analyzed as colloidal solutions after AAO elimination

Discussion

In contrast to the abundant literature on the elaboration of titania nanotubes and nanorods by means of AAO templates, and on some reports on the synthesis of titania-supported copper nanoparticles via refined alkoxide sol–gel process, no reports were found for copper-doped titania catalysts confined in an ordered matrix. Our results indicate that we succeeded in obtaining titania and copper-doped titania nanotubes inside the ordered pore array of AAO templates, with two deposition techniques imposing different nucleation and growth conditions. Both deposition techniques depend on the characteristics of the template to tune an homogeneous transition from nanotubes to nanorods at longer deposition times; they rendered polycrystalline material that is sensitive to the presence of metal salts in the sol–gel bath an apparently, with the commercial AAO attempted here, the array is a combination of nanotubes and nanorods at long deposition times. The presence of Cu slows down titania precipitation causing smaller crystallite sizes and thinner titania layers inside and outside AAO pores. Small titania crystals are indicative of the interaction between CuO and TiO_2 due to a high vacancy (surface defects) and/or large hydroxyl concentration (surface functionality) [29]. Although, there are reports in the literature regarding the formation of sheet-type structures in Zr-doped TiO_2 nanotubes synthesized at low acid/metal alkoxide ratios [33], the fact that both Cu-free and Cu-doped TiO_2 nanotubes were synthesized under the same H+/Ti ratio, make us believe that sheet formation is due to the lower stability in NaOH of Cu-doped TiO_2 caused by the abundant in situ intercalation of Cu^{2+} ions, instead of an ill-defined geometry during AAO-coating. Finally, the smaller crystallite size and superior chemical stability toward NaOH of Cu-doped titania nanotubes produced by the flow technique, suggest different growth mechanisms. The flow technique renders thicker deposits conformed of small crystallites (fast nucleation/slow growth), while the immersion technique favors the formation of nanotubes with thinner walls conformed of larger crystals (slow nucleation/fast growth). None of these microstructural differences manifest themselves as clear differences in the optical absorption spectra of the powders, although detailed studies are in progress to determine the optical properties of TiO_2-nanotube, TiO_2-nanorod, and TiO_2-nanotube-nanowire arrays. It is notorious though, the red-shift in the absorbance spectra of colloidal TiO_2 nanotubes when compared to the normal band gap of TiO_2 film. It cannot be explained by differences in particle size/geometry since it has also been reported for nontubular 18 nm colloidal TiO_2 particles [26]. The shift most likely reflect sensitization by defects in the network of TiO_2 (i.e., abundance of lower valence Ti states), which could be enhanced by local changes in Ti/O ratio in confined AAO environment.

Conclusions

The effect of copper addition in the microstructure of sol–gel TiO_2 supported on AAO membranes is reported. Two deposition methods based on immersion and flow techniques were used for the coating of the porous AAO membrane with TiO_2. We found that the presence of copper decreases the thickness and crystallite size of titania coatings, and causes its lower chemical stability toward NaOH, giving Cu-doped titania nanosheets. Titania and Cu-doped titania nanotubes analyzed as colloidal solutions show band gaps substantially shifted to the red in comparison to the direct band gap of near-spherical materials grown on Corning glass substrates, most likely due to TiO_2 network defects. These findings are relevant in the field of photocatalysis and solar energy conversion, where the combination of well-defined geometries, small particle size, and broader spectrum photoresponse, may contribute to the overall improvement of the devices.

Acknowledgements Financial support from Programa de Apoyo a Proyectos de Investigación e Innovación Tecnológica (PAPIIT-UNAM IN111106-3), Proyecto Universitario de Nanotecnología (PUNTA-UNAM), Consejo Nacional de Ciencia y Tecnología (CONACYT 49100), is gratefully acknowledged, as well as the fellowship (S. López-Ayala) provided by CONACYT-México. We thank R. Morán, P. Altúzar, and M.L. Román for technical assistance and XRD analyses.

References

1. Kuchibhatla SVNT, Karakoti AS, Bera D, Seal S (2007) Prog Mater Sci 52:699
2. Shankar KS, Raychaudhuri AK (2005) Mater Sci Eng C 25:738
3. Li XH, Liu WM, Li HL (2005) Appl Phys A 80:317
4. Bai J, Zhou B, Li L, Liu Y, Zheng Q, Shao J, Zhu X, Cai W, Liao J, Zou L (2008) J Mater Sci 43:1880. doi:10.1007/s10853-007-2418-8
5. Chen P-L, Kuo CT, Pan FM (2004) Appl Phys Lett 84:3889
6. Tian T, Xiao X-F, Liu R-F, She H-D, Hu X-F (2007) J Mater Sci 42:5539. doi:10.1007/s10853-006-1104-6
7. Turkevych I, Pihosh Y, Goto M, Kasahara A, Tosa M, Takehana SK, Takamasu T, Kido G, Koguchi N (2008) Thin Solid Films 516:2387
8. Quan X, Yang SG, Ruan XL, Zhao HM (2005) Environ Sci Technol 39:3770
9. Ghicov A, Tsuchiya H, Macak JM, Schmuki P (2005) Electrochem Commun 7:505
10. Paulose M, Shankar K, Yoriya S, Prakasam HE, Varghese OK, Mor GK, Latempa TA, Fitzgerald A, Grimes CA (2006) J Phys Chem B 110:16179
11. Mor GK, Varghese OK, Paulose M, Shankar K, Grimes CA (2006) Sol Energy Mater Sol Cell 90:2011

12. Slamet Nasution HW, Purnama E, Kosela S, Gunlazuardi J (2005) Catal Commun 6:313
13. Nomura N, Tagawa T, Goto S (1998) React Kinet Catal Lett 63:9
14. Morán-Pineda M, Castillo S, Asomoza M, Gómez R (2002) React Kinet Catal Lett 76:75
15. Lim TH, Jeong S-M, Kim S-D, Gyenis J (2000) React Kinet Catal Lett 71:223
16. Huang Ch, Liu X, Liu Y, Wang Y (2006) Chem Phys Lett 432:468
17. Xin B, Wang P, Ding D, Liu J, Ren Z, Fu H (2008) Appl Surf Sci 254:2569
18. Araña J, Peña Alonso A, Doña Rodríguez JM, Herrera Melián JA, González Díaz O, Pérez Peña J (2008) Appl Catal B 78:355
19. Zhu B, Zhang X, Wang S, Zhang S, Wu S, Huang W (2007) Microporous Mesoporous Mater 102:333
20. Kim K-H, Ihm S-K (2007) J Hazard Mater 146:610
21. Colón G, Maicu M, Hidalgo MC, Navío JA (2006) Appl Catal B 67:41
22. Xiaoyuan J, Guanghui D, Liping L, Yingxu C, Xiaoming Z (2004) J Mol Catal A 218:187
23. Tseng I-H, Wu JCS, Chou H-Y (2004) J Catal 221:432
24. Zhu Y-Q, Wen Y, Lai L-F, Zong F-Q, Wang J (2004) J Fuel Chem Technol 32:486
25. Qi G-X, Zheng X-M, Fei J-H, Hou Z-Y, Xu B, Dong L, Chen Y (1998) J Chem Soc Farad Trans 94:1905
26. Wu JCS, Seng I-H, Chang W-Ch (2001) J Nanopart Res 3:113
27. Patcas F, Krysmann W (2007) Appl Catal A 316:240
28. Yadlovker D, Berger S (2007) Sens Actuat B 126:277
29. Bokhimi X, Novaro O, Gonzalez RD, López T, Chimal O, Asomoza A, Gómez R (1999) J Solid State Chem 144:349
30. Guinier A (1994) In: Crystals, imperfect crystals, and amorphous bodies. Courier Dover, USA
31. Anderson MA, Gieselmann MJ, Xu Q (1988) J Membrane Sci 39:243
32. Perkowitz S (1993) Optical characterization of semiconductors: Infrared, Raman, and Photoluminescence spectroscopy. Academic Press Limited, London
33. Lucky RA, Charpentier PA (2008) Adv Mater 20:1755